Dimeric Transthyretin Variant Assembles into Spherical Neurotoxins†

Kimiaki Matsubara,‡Mineyuki Mizuguchi,*,‡ Kouhei Igarashi,‡ Yoshinori Shinohara,§ Makoto Takeuchi,‡ Atsushi Matsuura,‡ Takayuki Saitoh,‡ Yoshihiro Mori,‡ Hiroyuki Shinoda,‡ and Keiichi Kawano*,‡,||

Faculty of Pharmaceutical Sciences, Toyama Medical and Pharmaceutical University, Toyama 930-0194, Japan, and Faculty of Dental Science, Kyushu University, Fukuoka 812-8582, Japan

Received June 7, 2004; Revised Manuscript Received November 12, 2004

ABSTRACT: Familial amyloidotic polyneuropathy is a hereditary autosomal-dominant disease in which the deposited transthyretin fibrils are derived from amyloidogenic mutation. We investigated structure and stability of a human Ser112Ile transthyretin variant and showed that the Ser112Ile variant exists as a dimer having nonnative tertiary structure at physiological pH. In addition, the dimeric Ser112Ile assembles into a spherical aggregate and exerts cytotoxicity in a human neuroblastoma cell line. Our results suggest the importance of an unstable dimeric structure in forming spherical aggregates that will induce cell death.

Amyloidoses comprise a group of diseases in which some organ functions are destroyed as a result of deposits of fibrillar protein aggregates in extracellular spaces. Amyloid fibrils of various proteins generally consist of straight or curled fibrils 7.5−10 nm wide and up to several micrometers long. Amyloid fibrils of proteins share many structural characteristics, as discerned from X-ray diffraction pattern and electron and atomic force microscopy. Amyloid fibrils are known to possess the cross-β structure, which consists of continuous β-sheets lying parallel to the long axis of the fibril with the constituent β-strands running perpendicular to this axis. Moreover, amyloid fibrils bind thioflavin-T and Congo red with specific spectroscopic characteristics, implying unified structural properties (*1*−*4*). This characteristic feature is shared with more than 20 amyloidogenic proteins that cause various types of amyloidoses in humans. In addition, numerous proteins without connection to any known disease have been shown to be capable of forming amyloid fibrils in vitro under appropriate conditions (*5*, *6*).

Transthyretin (TTR)[1] is a homotetrameric β-sheet protein with a total molecular mass of 55 kDa and 127 amino acid residues/subunit, and is present in human plasma (3.6−7.2 μM) and cerebral spinal fluid (0.04−0.4 μM). The function of TTR is to transport a thyroid hormone (L-thyroxine, T4) and retinal, in the latter case through binding to retinol-binding protein (*7*, *8*). TTR is the major component of amyloid deposits in human tissue that putatively cause a wide range of amyloid diseases, including senile systemic amyloidosis (SSA) and familial amyloidotic polyneuropathy (FAP) (*9*, *10*). The wild-type TTR molecules are deposited as amyloid fibrils in SSA, a disorder that affects about 25% of individuals over 90 years old and sometimes leads to heart failure in the elderly. FAP is a hereditary autosomal-dominant disease in which the deposition of TTR-derived amyloid in these patients is strictly associated with point mutations in the coding region of the TTR gene. Currently, more than 80 different single-site mutants of TTR are known, and most of them are associated with FAP. Most individuals with FAP suffer from peripheral and autonomic nervous system dysfunction. TTR variants are also associated with familial amyloidotic cardiomyopathy, which leads to cardiac dysfunction (*11*−*13*).

The prevailing hypothesis regarding the property of TTR mutants to form fibrils is that various amino acid substitutions in TTR affect the stability of the tetramer and/or monomer and facilitate its conformational transition to an amyloidogenic intermediate having a nonnative tertiary structure capable of self-assembly (*14*−*17*). Although the TTR fibrils are strictly associated with FAP, the nature of the toxic structural species and the mechanism of cell damage are the subject of intense debate. Recent studies have suggested that the protein aggregates rather than the amyloid fibrils induce cell death, in some cases through an apoptosis-like mechanism (*18*−*22*). In this report, we describe the structure, stability, and toxicity of the pathogenic TTR variant with a Ser112 to Ile mutation (S112I-TTR). The clinical picture of S112I-TTR amyloidosis has been characterized by a sensorimotor neuropathy of the lower limbs, followed by the appearance of dysautonomy, severe cardiomyopathy, and chronic kidney failure (*23*). We demonstrated that S112I-TTR exists as a dimer with nonnative tertiary interactions. Interestingly, the S112I variant self-assembles into insoluble

† This study was supported by grants from the Ministry of Education, Culture, Sports, Science and Technology of Japan; by the Program for the Promotion of Basic Research Activities for Innovative Biosciences (Japan); by the National Project on Protein Structural and Functional Analyses; and by a grant from the Ministry of Agriculture, Forestry and Fisheries of Japan (Rice Genome Project PR-4101).

* Corresponding authors: Faculty of Pharmaceutical Sciences, Toyama Medical and Pharmaceutical University, 2630 Sugitani, Toyama 930-0194, Japan. (M.M.) Tel 81-76-434-7595; fax 81-76-434-5061; e-mail mineyuki@ms.toyama-mpu.ac.jp. (K.K.) Tel 81-76-434-5061; fax 81-76-434-5061; e-mail kawano@ms.toyama-mpu.ac.jp.

‡ Toyama Medical and Pharmaceutical University.

§ Kyushu University.

|| Present address: Division of Biological Sciences, Graduate School of Science, Hokkaido University, Sapporo 060-0810, Japan.

[1] Abbreviations: TTR, transthyretin; T4, L-thyroxine; SSA, senile systemic amyloidosis; FAP, familial amyloidotic polyneuropathy; CD, circular dichroism; SDS−PAGE, sodium dodecyl sulfate−polyacrylamide gel electrophoresis; ANS, 1-anilino-8-naphthalenesulfonate; Flu, flufenamic acid; AFM, atomic force microscopy; PBS, phosphate-buffered saline.

10.1021/bi048838c CCC: $30.25
Published on Web 02/10/2005

spherical aggregates under nearly physiological conditions, and it induces cell death in a human neuroblastoma cell line.

MATERIALS AND METHODS

Expression and Purification of TTR in E. coli. The expression plasmid for S112I-TTR was prepared with the plasmid of wild-type TTR as a template by use of the QuikChange site-directed mutagenesis procedure from Stratagene (*24*). The sequence of the inserted DNA segment was verified by DNA sequencing with the DNA sequencing kit (Applied Biosystems) with pQE30 sequencing primer (Qiagen). The plasmid was transformed into competent M15 cells (Qiagen). Wild-type TTR and S112I-TTR were expressed and purified as described (*24*).

Size-Exclusion Chromatography. A 24-mL column containing Sephadex G-75 (Superdex G-75, Amersham Pharmacia Biotech) connected to a Bio-Logic HR Basic system (Bio-Rad Laboratories) was equilibrated with 50 mM phosphate buffer containing 100 mM KCl and 1 mM EDTA (pH 7.0). The lyophilized protein was dissolved in the phosphate buffer solution and incubated at 4 °C for about 12 h before it was applied onto the column. All gel-filtration analyses were performed at 4 °C with a flow rate of 0.4 mL/min. The following proteins were used as molecular mass standards: albumin (69.8 kDa), ovalbumin (49.4 kDa), chymotrypsinogen A (21.2 kDa), and ribonuclease A (15.8 kDa).

Cross-Linking with Glutaraldehyde. Quaternary structure of wild-type TTR and S112I-TTR was evaluated by glutaraldehyde cross-linking as described previously (*22*, *25*). The lyophilized protein was dissolved in 50 mM phosphate buffer containing 100 mM KCl and 1 mM EDTA (pH 7.0) and incubated at 4 °C for about 12 h before 25% glutaraldehyde solution was added. The samples were boiled for 5 min before they were loaded onto a gel for sodium dodecyl sulfate−polyacrylamide gel electrophoresis (SDS−PAGE).

Circular Dichroism and Fluorescence Measurement. Samples for the equilibrium urea-induced unfolding were obtained as described previously (*26*). The protein concentration was 35 μM. The buffer solutions contained 50 mM phosphate, 100 mM KCl, and 1 mM EDTA (pH 7.0). The circular dichroism (CD) spectra were recorded on a Jasco J-805 spectropolarimeter (Jasco). Quartz cuvettes with 1- and 10-mm path lengths were used for the far- and near-UV experiments, respectively. All CD measurements were performed at 25 °C. Spectra were collected with a scan speed of 50 nm/min and with a response time of 1 s. Each spectrum was the average of two scans.

Fluorescence measurements were performed on a F-4500 fluorescence spectrometer (Hitachi). Samples were excited at 295 nm with a bandwidth of 1 nm to measure the tryptophan fluorescence. Fluorescence emission spectra were recorded from 300 to 450 nm with a bandwidth of 20 nm.

In the acrylamide quenching experiments, aliquots of 1 M acrylamide stock solution were added to a protein solution (35 μM) to achieve the desired acrylamide concentration. Excitation was set at 295 nm to excite tryptophan, and the emission spectrum was recorded in the range of 300−400 nm. Fluorescence intensities for the acrylamide quenching experiments were corrected by multiplying the measured intensity by a factor, $2.3A/(1 - 10^{-A})$, where A is the absorbance of a given concentration of acrylamide at 295 nm and 10-mm path-length.

We prepared 1-anilino-8-naphthalenesulfonate (ANS) solutions (30 μM) containing 50 mM phosphate, 100 mM KCl, and 1 mM EDTA (pH 7.0). The protein concentrations were 0.7 μM, and the protein solutions were incubated at 25 °C for 24 h. Fluorescence intensities were recorded with an excitation wavelength of 380 nm, and emission spectra were recorded from 400 to 600 nm. The bandwidths for excitation and emission were set to 10 and 20 nm, respectively.

Aggregation Assay. Protein solutions at 1.0 mg/mL protein concentration (10 mM phosphate, 100 mM KCl, and 1 mM EDTA, pH 7.5) were diluted 1:1 with a buffer containing 200 mM buffer solute, 100 mM KCl, and 1 mM EDTA at the desired pH. Citrate buffer was used when the final pH was below 5.4; phosphate buffer was employed at pH levels above 5.8. All samples were incubated at 37 °C for 72 h without stirring. Sample solutions were vortexed gently, and turbidity at 330 nm was measured.

Inhibition of aggregate formation was investigated by diluting a protein solution into citric buffer at pH 4.4. Stock solutions of T4 and flufenamic acid (Flu) were prepared by dissolving the T4 and Flu in dimethyl sulfoxide at 5 mM. Protein solution at 1.0 mg/mL (10 mM phosphate, 100 mM KCl, and 1 mM EDTA, pH 7.0) containing various concentrations of T4 or Flu was diluted 1:1 with citric acid buffer (200 mM citric acid, 100 mM KCl, and 1 mM EDTA, pH 4.4) (*17*, *27*). After the solutions were incubated at 37 °C for 72 h, turbidity at 330 nm was measured.

TTR aggregation was also evaluated by thioflavin-T binding as described (*2*, *26*). The suspension of insoluble TTR (400 μL) described above was mixed with 2.57 mL of a buffer (200 mM Tris, 100 mM KCl, and 1 mM EDTA at pH 8.0), together with 30 μL of a thioflavin-T stock solution (2.0 mM).

The time course of aggregation was monitored by measuring turbidity at 330 nm of TTR solutions at pH 7.0. Lyophilized TTRs were dissolved in buffer solutions containing 50 mM phosphate, 100 mM KCl, and 1 mM EDTA (pH 7.0) and filtered. The protein solutions were incubated at 37 °C without stirring before measurements.

Atomic Force Microscopy. We prepared solutions at 0.5 mg/mL protein concentration (10 mM phosphate, 100 mM KCl, and 1 mM EDTA, pH 7.0) and filtered. The solutions were incubated at 37 °C for periods up to 5 weeks. The incubated sample was gently mixed, and aliquots were taken out at 72 h, 168 h, and 5 weeks. A drop of each solution was placed on freshly cleaved mica and left at room temperature. Then the solution was rinsed with ultrapure water to remove loosely bound protein and dried. The atomic force microscopic (AFM) images were obtained on a multimode microscope with a Nanoscope IIIa (Digital Instruments, Santa Barbara, CA). Tapping-mode AFM was employed with standard etched-silicon probes. A radius of curvature (R_c) of the AFM tip was less than 10 nm.

Cell Culture. The human neuroblastoma cell line IMR-32 (IFO50283; Health Science Research Resources Bank) was cultured at 37 °C under a 5% CO_2 atmosphere in Eagle's minimum essential medium containing Earle's salts, 10% fetal calf serum, and 2 mM L-glutamine. Cells were plated onto culture flasks coated with collagen type I (BD Biosciences).

Toxicity Assays. IMR-32 cells were cultured in 4-well culture slides and incubated with wild-type TTR or S112I-TTR for 24 h. The protein solutions were prepared by dissolving the lyophilized samples in a phosphate-buffered saline (PBS) solution at final protein concentrations of 100 μM. The protein solutions were filtered and preincubated at 37 °C for 3 days before they were added to the cells. The protein solution (100 μL) was diluted with 0.9 mL of Eagle's minimum essential medium containing Earle's salts, 10% fetal calf serum, and 2 mM L-glutamine (final concentrations of proteins were 10 μM) and added to cells. The slides were washed with a PBS solution and exposed for 30 min to propidium iodide and Hoechst 33342. Reactions to each dye were detected with a fluorescent photomicroscope (Provis AX80, Olympus).

Toxicity was measured by determining ATP content with the ViaLight HS kit (Lumitech Ltd., Nottingham, U.K.) (*28*). The protein solutions at 100 μM concentrations were preincubated at 37 °C for 3 days and 10-fold diluted with the culture medium before the solutions were added to the cells. After 24 h of treatment with a protein, cytotoxicity was assayed by the ViaLight assay according to the manufacturer's instructions. The control value was obtained by adding PBS solution to cells.

RESULTS

Quaternary Structure. Quaternary structure was monitored by analytical gel-filtration chromatography. Figure 1A shows gel-filtration elution profiles of wild-type TTR and S112I variant in solutions at pH 7.0 and 4 °C. The chromatogram of wild-type TTR shows the presence of one peak with an elution volume of 9.5 mL, corresponding to a molecular mass of 60 kDa (tetramer). For S112I-TTR, a peak is observed with elution volumes around 10.4 mL, and the molecular mass is estimated to be 30 kDa. Therefore, S112I-TTR has a dimeric structure in neutral pH solution. The dimeric structure of S112I-TTR was confirmed by cross-linking technique (Figure 1B).

Gel-filtration column separates proteins by their hydrodynamic dimensions rather than by molecular masses. It is known that 15−20% increase in the hydrodynamic radius (which is typical for the protein in molten globule state) results in the 2-fold increase in the apparent molecular weight measured by a gel-filtration column calibrated by a set of native globular proteins. Therefore, the gel-filtration data alone cannot rule out the possibility that S112I-TTR is a molten-globule-like monomer whose hydrodynamic radius could explain a molecular weight corresponding to a dimer. However, this possibility was excluded on the basis of the chemical cross-linking data for S112I-TTR (Figure 1B).

Secondary and Tertiary Structures. To compare the secondary and tertiary structure of wild-type TTR and S112I-TTR, we performed far- and near-UV CD studies at pH 7.0 and 25 °C (Figure 2). Two characteristic positive near-UV CD peaks of the wild-type TTR, one at 283 nm and the other at 291 nm, indicate the presence of rigid packing interactions of aromatic side chains. Apart from the difference in intensity, the peak at 291 nm is also present in the spectrum of S112I-TTR. However, the peak at 283 nm is not clearly observed and a broad band is present around 260−285 nm in the spectrum of S112I-TTR. These results suggest that

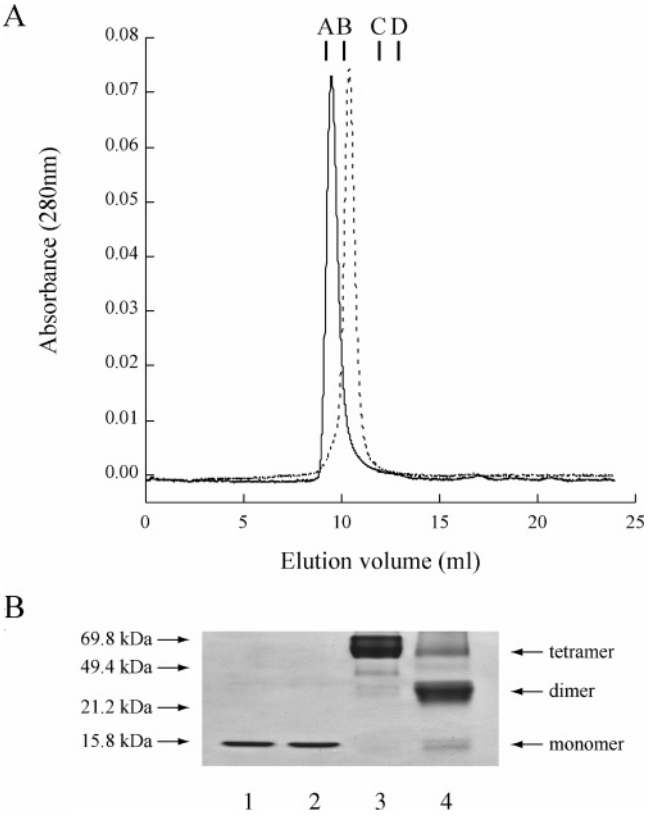

FIGURE 1: (A) Analytical size-exclusion chromatograms of wild-type TTR and S112I-TTR. Standard positions are indicated as follows: A, albumin (69.8 kDa); B, ovalbumin (49.4 kDa); C, chymotrypsinogen A (21.2 kDa); D, ribonuclease A (15.8 kDa). (B) SDS−PAGE of wild-type TTR (lanes 1 and 3) and S112I-TTR (lanes 2 and 4). The samples were boiled before they were applied onto the gel. Lanes 3 and 4 represent SDS−PAGE of proteins after cross-linking with glutaraldehyde.

the environment of aromatic side chains is changed by replacing the Ser112 with Ile. In the far-UV CD region, the spectrum of S112I-TTR is similar to that of wild-type TTR, indicating that these two proteins have similar levels of secondary structure at pH 7.0. A broad signal at around 215 nm is characteristic of β-sheet structure.

Conformational Stability. We investigated secondary and tertiary structural stabilities by monitoring the urea-induced unfolding at pH 7.0 and 25 °C. The urea-induced unfolding curves of wild-type TTR and the S112I variant are shown in Figure 3. The decrease of the CD ellipticity at 215 nm reflects the disruption of secondary structure by urea. The fluorescence intensity at 330 nm (I_{330}) decreased with increasing urea concentration, indicating the loss of specific side-chain packing interactions of Trp residues (*29*). There are two tryptophan residues in TTR, Trp41 and Trp79 (the latter is quenched in the folded state) (*16*). The midpoints (C_m) of the urea-induced unfolding curves were obtained as described previously (*30*, *31*) and are represented in Table 1. The urea-induced unfolding curves of wild-type TTR show cooperative transition, since disruption of the secondary structure is almost coincident with disruption of the tertiary structure (Figure 3A and Table 1). Nevertheless, the unfolding transition curve of S112I-TTR shows that secondary structure measured by CD ellipticities at 215 nm is disrupted first, followed by unfolding of the tertiary structure measured by Trp fluorescence (Figure 3B and Table 1). These data

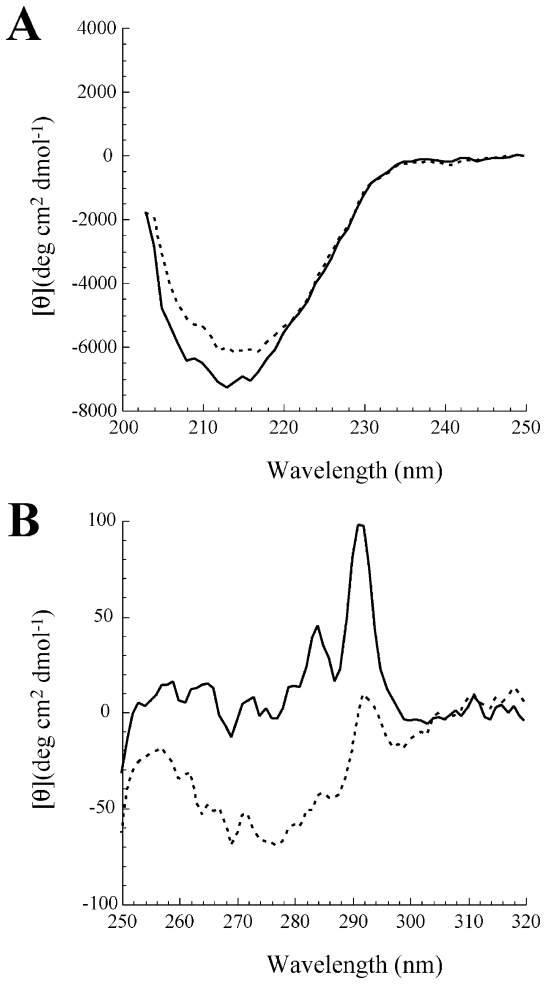

FIGURE 2: CD spectra of wild-type TTR (—) and S112I variant (---) in (A) far- and (B) near-UV regions (pH 7.0 and 25 °C).

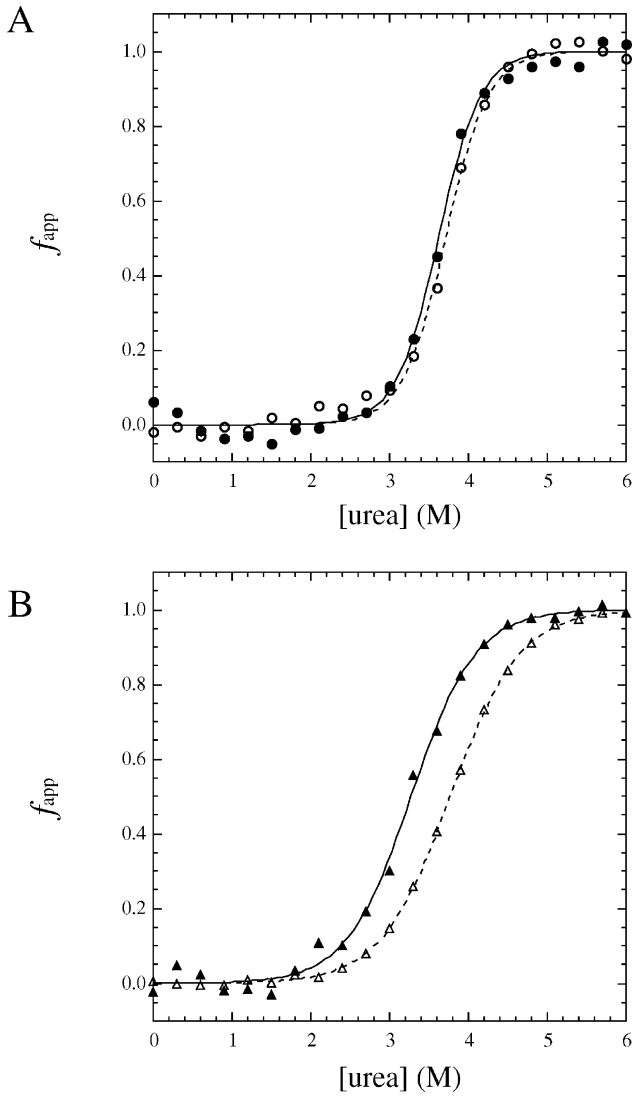

FIGURE 3: Urea-induced equilibrium unfolding curves of (A) wild-type TTR and (B) S112I-TTR measured by the CD ellipticities at 215 nm (solid symbols) and fluorescence intensity (I_{330}) (open symbols) at pH 7.0 and 25 °C. The apparent fractional extent of unfolding (f_{app}) was obtained from the CD, and the I_{330} values were obtained by the following equation: $f_{app} = (A_{obs} - A_1)/(A_2 - A_1)$, where A_1 and A_2 represent the baselines for the pre- and posttransition zones, respectively, and A_{obs} is the observed CD or I_{330} value.

suggest that noncoincident disruption of secondary and tertiary structure occurs in the unfolding of the S112I variant (*26*).

Acrylamide Quenching of Tryptophan Fluorescence. In a globular protein, the degree to which an amino acid side chain is exposed to solvent depends on how it is shielded from the solvent by the other parts of the protein molecule. The degree of exposure of Trp residues in solution was determined by an acrylamide quenching experiment (*32*, *33*). To compare the degree of exposure of Trp residues in wild-type TTR and S112I-TTR, we measured the Trp fluorescence intensities in the presence of acrylamide. Figure 4 shows the Stern−Volmer plots for wild-type TTR and S112I-TTR in the presence of 0−0.9 M acrylamide.

We analyzed the acrylamide quenching data according to the modified Stern−Volmer equation, $F_0/F = (1 + K_{SV}[Q])\exp(V[Q])$, where F_0 and F denote the fluorescence intensities in the absence and presence of acrylamide, respectively; [Q] is the concentration of quencher; and K_{SV} and V are the dynamic and static quenching constants, respectively (*32*, *33*). Stern−Volmer plots for wild-type TTR and S112I-TTR show similar positive slopes with dynamic quenching constants of 2.24 and 2.26 M^{-1}, respectively.

We also determined dynamic quenching constants for wild-type TTR and S112I-TTR in the presence of 6 M guanidinium chloride and obtained quenching constants of 4.04 and 4.19 M^{-1}, respectively (Figure 4). These values are greater than those for the native states, showing the existence of buried Trp residues in the native states of wild-type TTR and S112I-TTR. Therefore, the acrylamide quenching data indicate that the solvent accessibility of the Trp residues is identical between tetrameric wild-type TTR and dimeric S112I variant.

Table 1: Conformational Stabilities of Wild-Type TTR and S112I-TTR[a]

	C_m[b] (M)	C_m[c] (M)
wild-type TTR	3.62 ± 0.02	3.71 ± 0.02
S112I-TTR	3.28 ± 0.02	3.77 ± 0.01

[a] C_m values represent the midpoints of urea-induced unfolding curves. [b] Derived from the unfolding curves monitored by CD ellipticities at 215 nm. [c] Derived from the unfolding curves monitored by the fluorescence intensity at 330 nm (I_{330}).

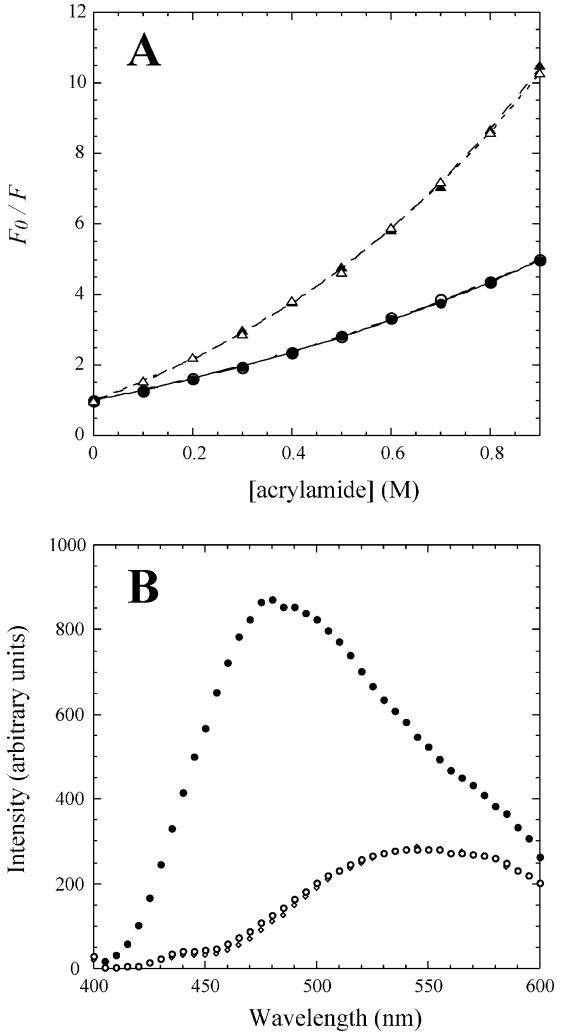

FIGURE 4: (A) Stern−Volmer plots of wild-type TTR (open symbols) and S112I-TTR (closed symbols) by acrylamide. F_0 and F designate the fluorescence intensities in the absence and presence of acrylamide, respectively. Circles and triangles denote the values of the proteins in the native and the unfolded state, respectively. (B) Fluorescence spectra of 30 μM ANS at pH 7.0 and 25 °C in the presence of wild-type TTR (●) and S112I-TTR (○). The protein concentrations were 6.6 μM. Diamonds represent the spectrum of 30 μM ANS at pH 7.0 and 25 °C in the absence of proteins. Excitation wavelength was 440 nm.

ANS Binding. The fluorescent hydrophobic molecule ANS is generally used as a probe for detecting solvent-exposed hydrophobic residues (*34*). It has been shown that two ANS molecules associate tightly to the T4-binding sites, located in the hydrophobic channels of wild-type tetrameric TTR in the native state, resulting in strong fluorescence intensity (*16*, *17*). The increase in fluorescence intensity and the shifts of the maximum wavelength from 550 to 478 nm are observed when ANS binds to wild-type TTR. On the contrary, the fluorescence spectra of ANS is not affected by adding S112I-TTR to the solution, indicating that the structure of the T4-binding site is changed by the S112I substitution (Figure 4B). The inability of S112I-TTR to bind to ANS was confirmed by monitoring the energy transfer from Trp to ANS (data not shown) (*16*).

Aggregation of Wild-Type TTR and S112I Variant. Aggregation of wild-type TTR and S112I-TTR at 37 °C as a function of pH was monitored by turbidity at 330 nm. The S112I variant formed more aggregates and exhibited a broader pH aggregation profile than did the wild-type TTR (Figure 5A). We also investigated the aggregation of TTR in the presence of T4 and Flu under acidic conditions (Figure 5C). Previous study has shown that T4 and Flu tightly bind to the hydrophobic channels of the TTR tetramer, resulting in a strong inhibition of TTR aggregation (*27*). Aggregation of wild-type TTR is almost completely inhibited in the presence of 16.5 μM inhibitor. The extent of the inhibition decreases as the concentration of inhibitor is decreased. However, the inhibitory effects of T4 and Flu are not observed for S112I-TTR (Figure 5C).

Aggregation of TTR was also investigated by monitoring thioflavin-T fluorescence (*2*, *26*). Aggregates of TTR enhance the fluorescence intensity of thioflavin-T, indicating the presence of amyloid-like structures in these aggregates. S112-TTR formed more amyloid-like structure than did the wild-type TTR at pH 4.2 and 4.6 (Figure 5B). Thioflavin-T fluorescence data also show that T4 and Flu clearly inhibit the aggregation of wild-type TTR, but these inhibitors do not inhibit the aggregation of S112I-TTR (Figure 5D).

AFM Images of S112I Aggregates. Aggregations of TTRs under physiological conditions were investigated by turbidity at 330 nm. Figure 6A shows the time course of TTR aggregations at 37 °C and pH 7.0. S112I-TTR formed small but significant amounts of aggregates after long incubation, while wild-type TTR does not. We used AFM to evaluate the morphology of S112I aggregates under physiological conditions. After 3 days of incubation, S112I-TTR solutions were completely fibril-free, exclusively comprising small spherical aggregates and large amorphous aggregates (Figure 6B). Interestingly, the morphological feature of small spherical aggregates of S112I-TTR is similar to the morphology of Aβ nonfibrillar aggregates named Aβ-derived diffusible ligands or Aβ spherical aggregates (amylospheroid) (*20*, *35*). The Aβ spherical aggregates with *Z*-height of 2−5 nm determined by AFM correspond to 10−100-kDa particles (*35*, *36*). The AFM *Z*-height measurements gave an average height of 7.9 nm (range 4.4−9.8 nm) for the small spherical aggregates of S112I-TTR, with an average width of 34.1 nm (range 28.9−42.5 nm) (Figure 6B). It should be noted that the measured *Z*-height value by AFM tends to underestimate the actual molecular height due to physical compression exerted by the AFM probe (*36*), whereas shape of the AFM chip contributes to an overestimation of lateral feature size. When the AFM tip with a radius of curvature (R_c) is used, the width (W) of the imaged biomolecule is given as (*37*)

$$W \approx 4(R_m R_c)^{1/2}$$

where R_m is the radius of the molecule. From the equation, an average diameter was estimated to be 14.6 nm, and an average volume of the spherical aggregates was 1630 nm^3. No fibrils were observed after the long incubation of the S112I-TTR solution at 37 °C for 5 weeks (Figure 6C).

S112I-TTR Is Cytotoxic to IMR-32 Neuroblastoma Cells. We analyzed whether S112I-TTR is cytotoxic to IMR-32 cells. Control cells were not reactive to propidium iodide, a marker of cell death (Figure 7A). On the contrary, 24-h exposure of these cells to the S112I-TTR solution at pH 7.0 resulted in reaction to propidium iodide, whereas the wild-type TTR solution at pH 7.0 had no effect on IMR-32. The S112I-TTR and wild-type TTR solutions were preincubated

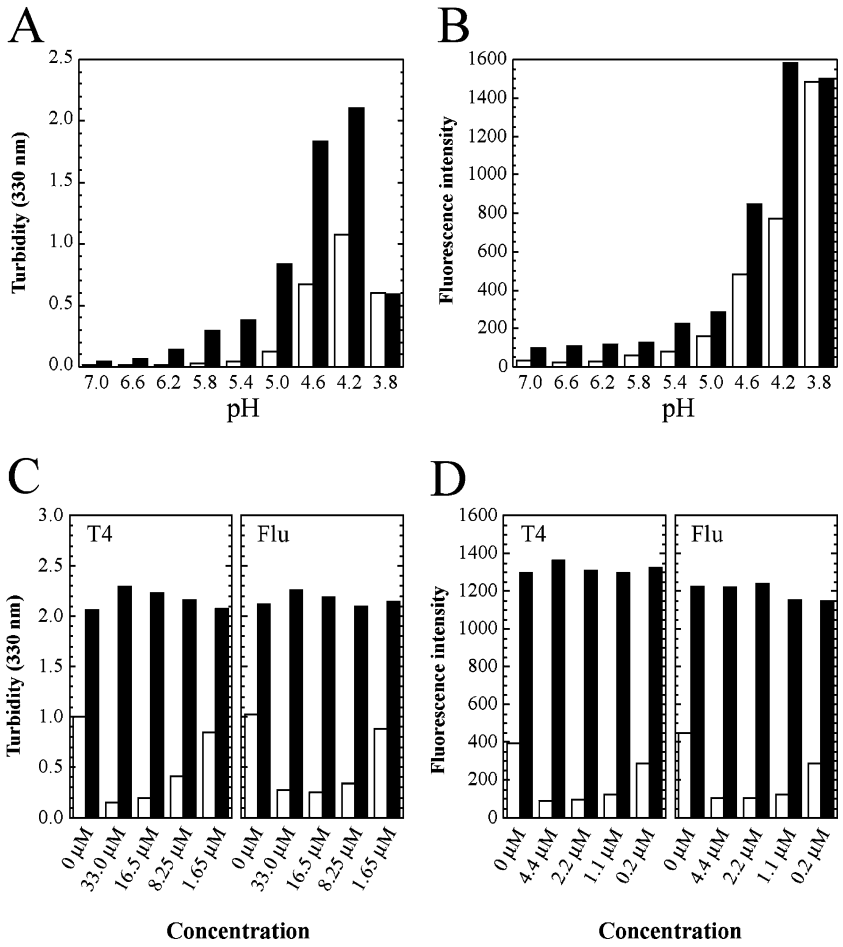

FIGURE 5: Aggregations of wild-type TTR (open bars) and S112I-TTR (solid bars). (A, B) pH dependence of aggregations monitored by turbidity at 330 nm (A) and by thioflavin-T fluorescence (B). (C, D) Aggregations of TTR at pH 4.4 monitored by turbidity at 330 nm (C) and by thioflavin-T fluorescence (D) in the presence of various concentrations of T4 or Flu. (A, C) Final protein concentrations are 33 μM; (B, D) final protein concentrations are 4.4 μM.

at 37 °C for 3 days before they were added to the cells. Hoechst 33342 stains nuclei of cells blue, and a clear blue spot indicates condensation of nuclei, which is a late marker of apoptosis. Cells treated with S112I-TTR show the clear blue spot (Figure 7A). These data indicate that the preincubated S112I induces neuronal cell death, likely apoptosis.

We determined the viability of IMR-32 cells treated with wild-type TTR and S112I-TTR, using ATP levels as an indicator of cell viability. The S112I-TTR significantly reduced neuronal viability, while preincubated wild-type TTR had no effect on cell viability (Figure 7B). The AFM imaging revealed that the S112I variant formed abundant spherical aggregates after the solution was incubated for 3 days at pH 7.0 and 37 °C (Figure 6). Taken together, these data suggest that the spherical aggregates of the S112I variant participate in cell death as a toxin.

We investigated the toxicity of the aggregates formed in a citrate buffer at pH 4.4. The aggregates formed at pH 4.4 substantially enhance the fluorescence intensity of thioflavin-T, indicating the presence of amyloid-like structures in these aggregates (Figure 5). The protein solution containing 10 μM wild-type TTR or S112I-TTR were incubated at pH 4.4 and 37 °C for 3 days. The aggregates were collected by centrifugation and resuspended in PBS solution. After the aggregate suspension was diluted 10-fold with the culture medium, IMR-32 cells were exposed to the suspension of the aggregates, and cell viability was measured as described under Materials and Methods. The suspension of the aggregates formed at pH 4.4 showed no effect on cell viability, indicating that the aggregates formed at pH 4.4 are not toxic to IMR-32 cells.

DISCUSSION

Protein aggregates, including amyloid fibrils, have been the target of increasing attention because of their central role in several human pathologies, including Alzheimer's disease, Parkinson's disease, and TTR amyloidoses. To intervene in these debilitating diseases linked to protein aggregation and deposition, it is essential to understand the structural changes of proteins leading to protein aggregation. In this study, we have shown that the S112I variant has dimeric structure with nonnative side-chain interactions at physiological pH. In addition, S112I-TTR is an unstable molecule, which easily aggregates and has a toxic effect on the neuroblastoma cell line.

Our data indicate that the tertiary structure of the dimeric S112I-TTR differs from that of the native tetrameric structure, although the secondary structures of wild-type TTR and S112I-TTR are similar to each other (Figure 2). The intensities of positive peaks at 283 and 291 nm are decreased by the S112I mutation, implying that the S112I variant has a poorly defined tertiary structure. However, the solvent accessibility of Trp is not changed by the S112I mutation as

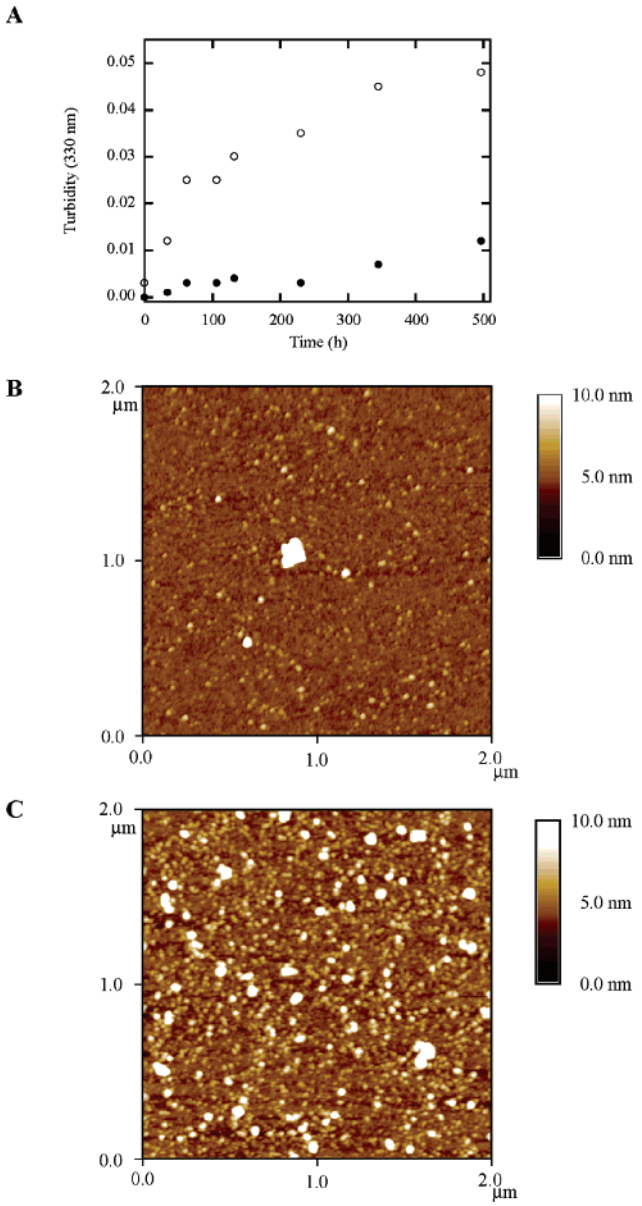

FIGURE 6: (A) Time course of aggregations of wild-type TTR (●) and S112I-TTR (○) at pH 7.0 and 37 °C. Aggregations were monitored by turbidity at 330 nm. (B, C) AFM images of S112I-TTR aggregates (10 nm total *Z*-range). AFM images show small spherical aggregates and large irregularly shaped amorphous aggregates. A solution containing 0.5 mg/mL S112I-TTR was incubated at pH 7.0 and 37 °C for (B) 72 h and (C) 5 weeks.

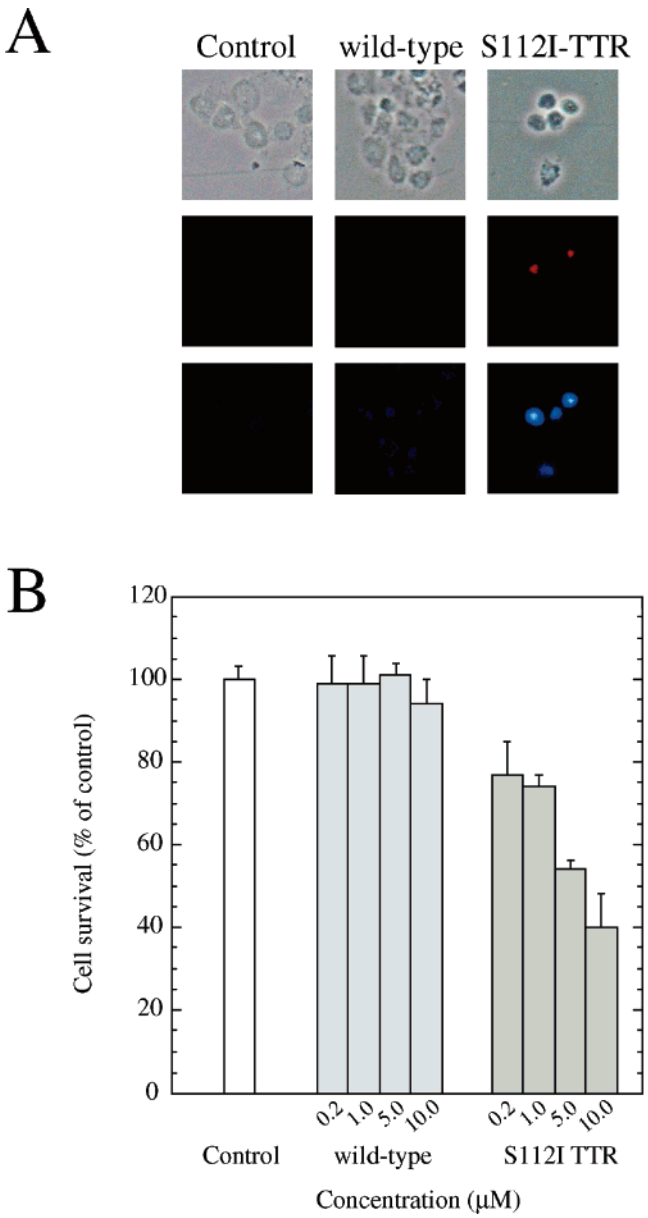

FIGURE 7: (A) IMR-32 cells treated with preincubated wild-type TTR or S112I-TTR (top). After the 24-h treatments, cultures were stained with propidium iodide (middle) and Hoechst 33342 (bottom). (B) Viability of IMR-32 cells after exposure to wild-type TTR or S112I-TTR. IMR-32 cells were plated at 1000 cells/well and incubated for 24 h with wild-type TTR or S112I-TTR at various concentrations indicated. Cell viability was measured by determining ATP content, with the ViaLight assay kit.

monitored by the acrylamide quenching experiment (Figure 4). These data indicate that the S112I variant has nonnative tertiary structure at physiological pH. The stability of the secondary and tertiary structure is not largely affected by the S112I mutation, since the C_m values derived from the far-UV CD and Trp fluorescence are similar between wild-type TTR and S112I-TTR (Figure 3 and Table 1). However, the cooperativity of the unfolding is changed by the S112I mutation as judged by the noncoincidence of the unfolding curves by CD and fluorescence (*26*, *30*).

The quaternary structure of TTR is substantially destabilized by the S112I mutation. Analytical gel filtration data show that S112I-TTR has a dimeric structure at pH 7.0 and 4 °C, even though wild-type TTR retains the native tetrameric structure under the same experimental conditions. The inability of S112I-TTR to assemble into the tetramer is responsible for disruption of the T4-binding channels, since the T4-binding channels of TTR are formed by an assembly of the four monomer subunits (*11*). T4 and Flu stabilize the quaternary structure and inhibit aggregation of wild-type TTR. In the case of S112I-TTR, the T4 and Flu had no effect on aggregation (Figure 5). These data are consistent with the ANS fluorescence experiments, showing that the ANS molecule does not bind to S112I-TTR (Figure 4). T4, Flu, and ANS bind to the hydrophobic channels formed by the association of the four monomer subunits. Our results indicate that a small molecule drug like Flu is not efficacious as a therapeutic in the case of S112I-TTR amyloidosis.

The destabilization of native quaternary conformation renders the TTR molecule more prone to form spherical aggregates under physiological conditions (Figure 6). The

native conformation of wild-type TTR has no tendency to aggregate under physiological conditions, since the four monomer subunits bind tightly through the hydrophobic and electrostatic interactions (*14*, *16*). However, the dimeric structure of S112I-TTR appears to lose dimer−dimer interactions, providing an opportunity for intermolecular interactions causing spherical aggregate formation to take place at physiological pH. The dimeric quaternary structure leads to formation of the spherical aggregates but not to amyloid fibril formation at physiological pH, since the S112I-TTR solution is completely fibril-free after prolonged incubation at pH 7.0 and 37 °C (Figure 6C). A number of studies have suggested that a monomeric amyloidogenic intermediate is required for the amyloid fibril formation of TTR (*14*−*17*), but our data show that the spherical aggregates are formed at physiological pH from dimeric molecular species with nonnative tertiary interactions (Figures 1 and 6).

Recent studies have focused on the importance of oligomeric aggregates as major cytotoxic species in various types of amyloidoses (*18*−*22*). Moreover, the inherent toxicity of aggregated proteins not associated with amyloidosis has been demonstrated (*6*). Interestingly, the small spherical aggregates of S112I-TTR are similar to Aβ nonfibrillar aggregates shown in previous studies (*20*, *35*). In Alzheimer's disease, recent in vivo as well as in vitro studies support the toxicity of nonfibrillar oligomers and their possible causative role in neuropathology (*6*, *18*−*20*). Here, we have shown that the S112I variant, probably the spherical aggregate of this protein, induces cell death in the human neuroblastoma cell line through an apoptosis-like mechanism (Figures 6 and 7). Sousa et al. (*38*, *39*) have demonstrated that the aggregated nonfibrillar form of TTR is deposited in an early stage of FAP before amyloid fibril deposition. The small spherical aggregates of TTR may be the cytotoxic molecular species in the early stage of FAP.

ACKNOWLEDGMENT

We thank Dr. Tsuneo Imanaka for helpful discussions and Dr. Ken-ichiro Mitsui for technical assistance.

REFERENCES

1. Glenner, G. G. (1980) Amyloid deposits and amyloidosis. The beta-fibrilloses, *N. Engl. J. Med. 302*, 1283−1292.
2. Naiki, H., Higuchi, K., Hosokawa, M., and Takeda, T. (1989) Fluorometric determination of amyloid fibrils in vitro using the fluorescent dye, thioflavin T1, *Anal. Biochem. 177*, 244−249.
3. Lansbury, P. T. (1992) In pursuit of the molecular structure of amyloid plaque: new technology provides unexpected and critical information, *Biochemistry 31*, 6865−6870.
4. Sunde, M., Serpell, L. C., Bartlam, M., Fraser, P. E., Pepys, M. B., and Blake, C. C. (1997) Common core structure of amyloid fibrils by synchrotron X-ray diffraction, *J. Mol. Biol. 273*, 729−739.
5. Guijarro, J. I., Sunde, M., Jones, J. A., Campbell, I. D., and Dobson, C. M. (1998) Amyloid fibril formation by an SH3 domain, *Proc. Natl. Acad. Sci. U.S.A. 95*, 4224−4228.
6. Bucciantini, M., Giannoni, E., Chiti, F., Baroni, F., Formigli, L., Zurdo, J., Taddei, N., Ramponi, G., Dobson, C. M., and Stefani, M. (2002) Inherent toxicity of aggregates implies a common mechanism for protein misfolding diseases, *Nature 416*, 507−511.
7. Blake, C. C., Geisow, M. J., Swan, I. D., Rerat, C., and Rerat, B. (1974) Structure of human plasma prealbumin at 2−5 A resolution. A preliminary report on the polypeptide chain conformation, quaternary structure and thyroxine binding, *J. Mol. Biol. 88*, 1−12.
8. Blake, C. C., Geisow, M. J., Oatley, S. J., Rerat, B., and Rerat, C. (1978) Structure of prealbumin: secondary, tertiary and quaternary interactions determined by Fourier refinement at 1.8 A, *J. Mol. Biol. 121*, 339−356.
9. Saraiva, M. J., Birken, S., Costa, P. P., and Goodman, D. S. (1984) Amyloid fibril protein in familial amyloidotic polyneuropathy, Portuguese type. Definition of molecular abnormality in transthyretin (prealbumin), *J. Clin. Invest. 74*, 104−119.
10. Saraiva, M. J., Costa, P. P., and Goodman, D. S. (1988) Transthyretin (prealbumin) in familial amyloidotic polyneuropathy: genetic and functional aspects, *Adv. Neurol. 48*, 189−200.
11. Eneqvist, T., and Sauer-Eriksson, A. E. (2001) Structural distribution of mutations associated with familial amyloidotic polyneuropathy in human transthyretin, *Amyloid 8*, 149−168.
12. Connors, L. H., Richardson, A. M., Theberge, R., and Costello, C. E. (2000) Tabulation of transthyretin (TTR) variants as of 1/1/2000, *Amyloid 7*, 54−69.
13. Hund, E., Linke, R. P., Willig, F., and Grau, A. (2001) Transthyretin-associated neuropathic amyloidosis. Pathogenesis and treatment, *Neurology 56*, 431−435.
14. Colon, W., and Kelly, J. W. (1992) Partial denaturation of transthyretin is sufficient for amyloid fibril formation in vitro, *Biochemistry 31*, 8654−8660.
15. McCutchen, S. L., Colon, W., and Kelly, J. W. (1993) Transthyretin mutation Leu-55-Pro significantly alters tetramer stability and increases amyloidogenicity, *Biochemistry 32*, 12119−12127.
16. Lai, Z., Colon, W., and Kelly, J. W. (1996) The acid-mediated denaturation pathway of transthyretin yields a conformational intermediate that can self-assemble into amyloid, *Biochemistry 35*, 6470−6482.
17. Jiang, X., Smith, C. S., Petrassi, H. M., Hammarstrom, P., White, J. T., Sacchettini, J. C., and Kelly J. W. (2001) An engineered transthyretin monomer that is nonamyloidogenic, unless it is partially denatured, *Biochemistry 40*, 11442−11452.
18. Walsh, D. M., Klyubin, I., Fadeeva, J. V., Cullen, W. K., Anwyl, R., Wolfe, M. S., Rowan, M. J., and Selkoe, D. J. (2002) Naturally secreted oligomers of amyloid beta protein potently inhibit hippocampal long-term potentiation in vivo, *Nature 416*, 535−539.
19. Hartley, D. M., Walsh, D. M., Ye, C. P., Diehl, T., Vasquez, S., Vassilev, P. M., Teplow, D. B., and Selkoe, D. J. (1999) Protofibrillar intermediates of amyloid beta-protein induce acute electrophysiological changes and progressive neurotoxicity in cortical neurons, *J. Neurosci. 19*, 8876−8884.
20. Hoshi, M., Sato, M., Matsumoto, S., Noguchi, A., Yasutake, K., Yoshida, N., and Sato, K. (2003) Spherical aggregates of beta-amyloid (amylospheroid) show high neurotoxicity and activate tau protein kinase I/glycogen synthase kinase-3beta, *Proc. Natl. Acad. Sci. U.S.A. 100*, 6370−6375.
21. Andersson, K., Olofsson, A., Nielsen, E. H., Svehag, S. E., and Lundgren, E. (2002) Only amyloidogenic intermediates of transthyretin induce apoptosis, *Biochem. Biophys. Res. Commun. 294*, 309−314.
22. Reixach, N., Deechongkit, S., Jiang, X., Kelly, J. W., and Buxbaum, J. N. (2004) Tissue damage in the amyloidoses: Transthyretin monomers and nonnative oligomers are the major cytotoxic species in tissue culture, *Proc. Natl. Acad. Sci. U.S.A. 101*, 2817−2822.
23. De Lucia, R., Mauro, A., Di Scapio, A., Buffo, A., Mortara, R., Orsi, L., and Schiffer, D. (1993) A new mutation on the transthyretin gene (Ser112 to Ile) causes an amyloid neuropathy with severe cardiac impairment, *Clin. Neuropathol. 12*, S44.
24. Matsubara, K., Mizuguchi, M., and Kawano, K. (2003) Expression of a synthetic gene encoding human transthyretin in *Escherichia coli*, *Protein Expression Purif. 30*, 55−61.
25. Hammarström, P., Jiang, X., Deechongkit, S., and Kelly, J. W. (2001) Anion shielding of electrostatic repulsions in transthyretin modulates stability and amyloidosis: insight into the chaotrope unfolding dichotomy, *Biochemistry 40*, 11453−11459.
26. Shinohara, Y., Mizuguchi, M., Matsubara, K., Takeuchi, M., Matsuura, A., Aoki, T., Igarashi, K., Nagadome, H., Terada, Y., and Kawano, K. (2003) Biophysical analyses of the transthyretin variants, Tyr114His and Tyr116Ser, associated with familial amyloidotic polyneuropathy, *Biochemistry 42*, 15053−15060.
27. Miroy, G. J., Lai, Z., Lashuel, H. A., Peterson, S. A., Strang, C., and Kelly, J. W. (1996) Inhibiting transthyretin amyloid fibril formation via protein stabilization, *Proc. Natl. Acad. Sci. U.S.A. 93*, 15051−15056.

28. McCafferty, A. C., and Cree, I. A. (1994) Measurement of cell migration stimulated by interleukin 8: use of ATP chemiluminescence, *Cytokine 6*, 450−453.
29. Sommers, P. B., and Kronman, M. J. (1980) Comparative fluorescence properties of bovine, goat, human and guinea pig alpha lactalbumin. Characterization of the environments of individual tryptophan residues in partially folded conformers, *Biophys. Chem. 11*, 217−232.
30. Kuwajima, K., Nitta, K., Yoneyama, M., and Sugai, S. (1976) Three-state denaturation of alpha-lactalbumin by guanidine hydrochloride, *J. Mol. Biol. 106*, 359−373.
31. Santoro, M. M., and Bolen, D. W. (1988) Unfolding free energy changes determined by the linear extrapolation method. 1. Unfolding of phenylmethanesulfonyl alpha-chymotrypsin using different denaturants, *Biochemistry 27*, 8063−8068.
32. Eftink, M. R., and Ghiron, C. A. (1976) Exposure of tryptophanyl residues in proteins. Quantitative determination by fluorescence quenching studies, *Biochemistry 15*, 672−680.
33. Eftink, M. R., and Ghiron, C. A. (1981) Fluorescence quenching studies with proteins, *Anal. Biochem. 114*, 199−227.
34. Semisotnov, G. V., Rodionova, N. A., Razgulyaev, O. I., Uversky, V. N., Gripas', A. F., and Gilmanshin, R. I. (1991). Study of the "molten globule" intermediate state in protein folding by a hydrophobic fluorescent probe, *Biopolymers 31*, 119−128.
35. Dahlgren, K. N., Manelli, A. M., Stine, W. B., Baker, L. K., Krafft, G. A., and Ladu, M. J. (2002) Oligomeric and fibrillar species of amyloid-beta peptides differentially affect neuronal viability, *J. Biol. Chem. 277*, 32046−32053.
36. Huang, T. H., Yang, D. S., Plaskos, N. P., Go, S., Yip, C. M., Fraser, P. E., and Chakrabartty, A. (2000) Structural studies of soluble oligomers of the Alzheimer beta-amyloid peptide, *J. Mol. Biol. 297*, 73−87.
37. Vesenka, J., Guthold, M., Tang, C. L., Keller, D., Delaine, E., and Bustamante, C. (1992) Substrate preparation for reliable imaging of DNA molecules with the scanning force microscope, *Ultramicroscopy 42−44*, 1243−1249.
38. Sousa, M. M., Cardoso, I., Fernandes, R., Guimaraes, A., and Saraiva, M. J. (2001) Deposition of transthyretin in early stages of familial amyloidotic polyneuropathy: evidence for toxicity of nonfibrillar aggregates, *Am. J. Pathol. 159*, 1993−2000.
39. Sousa, M. M., Fernandes, R., Palha, J. A., Taboada, A., Vieira, P., and Saraiva, M. J. (2002) Evidence for early cytotoxic aggregates in transgenic mice for human transthyretin Leu55Pro, *Am. J. Pathol. 161*, 1935−1948.

BI048838C